Structure of a Prototypic Ionic Liquid: Ethyl-methylimidazolium Bromide

Bachir Aoun,[†,‡] Andreas Goldbach,[§] Shinji Kohara,[∥] Jean-François Wax,[⊥] Miguel A. González,[†] and Marie-Louise Saboungi*[,‡]

Institut Laue Langevin, 6 rue Jules Horowitz, BP 156, 38042 Grenoble Cedex 9, France, Centre de Recherche sur la Matière Divisée, CNRS-Université d'Orléans, 1b rue de la Férollerie, 45071 Orléans, France, Dalian Institute of Chemical Physics, 457 Zhongshan Road, 116023 Dalian, P. R. China, Japan Synchrotron Radiation Research Institute, 1-1-1 Kouto, Sayo-cho, Sayo-gun, Hyogo 679-5198, Japan, and Laboratoire de Physique des Milieux Denses, Université Paul Verlaine-Metz, 1, Boulevard F. D. Arago, 57078 Metz Cedex 3, France

Received: July 28, 2010

High-energy X-ray diffraction measurements have been carried out on 1-ethyl-3-methylimidazolium bromide and complemented with molecular-dynamics simulations. Because the structure of the corresponding crystal is known, both the liquid and the crystal phases are simulated numerically. The liquid structure factor is dominated by an intense peak at 1.7 $Å^{-1}$, associated mainly with the packing of the anions around the large cations. Analysis of the real-space correlations of the liquid shows that the Br^- ions are distributed more symmetrically around the cation ring and move closer to the ring atoms compared with the crystal. Although the distribution of the anions around the cation in the first coordination shell of the liquid exhibits clear analogies with the crystal, the cation−cation partial distribution function of the liquid shows a significant component with lower distances between ring centers, with some pairs coming as close as 3.5 Å in either parallel or antiparallel configurations. Finally, the presence of topological short-range order and charge ordering in the liquid is clearly demonstrated.

Introduction

Low-melting organic salts are attracting widespread attention because of potential applications as solvents in chemical reaction and separation technology and electrolytes in photovoltaic and fuel cells. They are usually formed by pairing large, asymmetrically substituted cations such as the tetraalkylammonium, *N*-alkylpyridinium, or *N*,*N*-dialkylimidazolium ions with halide ions, symmetrical polyfluorides such as BF_4^- and PF_6^-, or large, asymmetric entities such as the bis(trifluoromethanesulfonyl)imide (TFSI) anion. The physicochemical properties of these so-called room-temperature ionic liquids (RTILs) are of particular interest, because they are the key to understanding the distinct and widely variable characteristics of RTILs.[1] In spite of the large number of experimental and theoretical studies that have appeared in the literature in the past 10 years, the understanding of the properties of RTILs at a molecular level remains a great challenge because of the complexity of their intermolecular interactions.[2] The most fundamental property at a microscopic level is the local arrangement of the molecules in the liquid, and in recent years, a large number of computational investigations have addressed the problem of determining the molecular structure of RTILs (see ref 3 and references therein). Those simulation studies predict specific structural features such as ion distributions, anion ordering on intermediate length scales, formation of nonpolar domains due to tail aggregation of cations, and variable molecular alignments at surfaces and interfaces. However, their results depend strongly on the force-field employed[4] and should be validated by comparison with experimental data.

Unfortunately, it is very difficult to probe experimentally the bulk structure of RTILs because of the large number of atoms involved and the broad distance distributions present in the liquid. Thus, although the number of laboratory studies which target local structural aspects at a molecular level employing, for example, NMR, Raman and IR spectroscopy are abundant, few experimental results on the short- and intermediate-range order of these complex organic liquids by X-ray or neutron scattering techniques have been reported. Among those, the most detailed study was carried out by Hardacre et al.,[5] who investigated the structure of the model RTIL 1,3-dimethylimidazolium (dmim) chloride by neutron diffraction with isotopic substitution, combined with a computational analysis of the experimental data. They showed the existence of significant charge ordering in this liquid, as well as some qualitative similarities between the liquid and the crystalline structures of this compound. They also investigated the structure of the salts formed by hexafluorophosphate (PF_6)[6] and bis(trifluoromethanesulfonyl)amide (NTf_2) with dmim.[7] Although the former is comparable to the structure of [dmim]Cl and resembles to some extent that of the crystal, the latter shows little similarity with the structure of the corresponding crystal phase, a behavior attributed to the conformational flexibility of the anion.[7] The existence of local structures in the liquid reminiscent of those in the crystalline phase has also been proposed from the analysis of Raman and X-ray diffraction data taken on 1-butyl-3-methyl (bmim) chloride and [bmim]Br[8] and [bmim]I.[9] Similarly, the main diffraction peak observed in a series of alkylimidazolium fluorohydrogenate RTILs studied by high-energy X-ray diffraction has been correlated with the layer structure of the crystal.[10,11] Triolo et al. also found a substantial degree of order in the amorphous states of [bmim][PF_6],[12] as well as a complex crystal

* To whom correspondence should be addressed. E-mail: saboungi@cnrs-orleans.fr.
[†] Institut Laue Langevin.
[‡] CNRS-Université d'Orléans.
[§] Dalian Institute of Chemical Physics.
[∥] Japan Synchrotron Radiation Research Institute.
[⊥] Université Paul Verlaine-Metz.

10.1021/jp1070715
Published on Web 09/16/2010

polymorphism that seems to be very common in RTILs.[8,13] Another characteristic feature of the structure of RTILs is the existence of a large degree of intermediate-range order in the liquid due to the separation of polar and nonpolar domains in RTILs with large neutral chains. This was suggested initially from simulation results[14−16] and confirmed later by Triolo et al. by means of X-ray diffraction on a series of alkylmethylimidazolium salts with different chain lengths.[17] As mentioned above, the large number and complexity of the intermolecular interactions prevents the possibility to derive detailed structural models of the liquid phase from X-ray or neutron-diffraction measurements alone, even when both are combined. However, with a combination of experiment and simulation, it becomes possible to obtain detailed insight into the local organization of RTILs. Takahashi et al. performed a neutron-diffraction experiment on chloroaluminate ionic liquids (MemIC−$AlCl_3$) and discussed the anion−cation correlations with the aid of an ab initio quantum-chemistry simulation.[18] Fujii et al. matched MD simulations with in-house X-ray scattering measurements of [emim]TFSI to focus on conformational changes of anion and cation in the liquid.[19] They find that, in this case, the crystal structure is largely modified in the liquid due to the existence of two conformers of the anion, whereas only one is present on the crystal. The role of the conformational isomerism of the cation in determining the spatial distribution around the anion has also been demonstrated by combining X-ray measurements on [emim]BF_4 with MD simulations.[20]

Here, we report high-energy X-ray diffraction (HEXRD) measurements on 1-ethyl-3-methylimidazolium bromide complemented with molecular-dynamics (MD) simulations. Because the crystalline structure of [emim]Br is known,[21] we simulate both liquid and crystal and explore the local similarities between the two phases. The Br^- ion has a relatively large X-ray form factor; therefore, the structural features related to the distribution of the anion around the cation and the anion−anion correlations at larger distances can be identified. Finally, high-energy X-rays allow measurements up to high momentum transfer Q ($= 4\pi \sin\theta/\lambda$; 2θ, scattering angle; λ, wavelength), making it possible to achieve high real-space resolution in the Fourier transform of the structure factor $S(Q)$.

Experimental Details

The starting material, [emim]Br (ACROS, 99.0%), was dried under high vacuum at 363 K for 24 h. After cooling, it was transferred to an Ar-filled glovebox, where samples were loaded into quartz capillaries with 1 mm outer diameter. The filled capillaries were under Ar reconnected to a vacuum line, heated above the melting point of [emim]Br (ca. 353 K), and carefully evacuated before being flame-sealed. HEXRD experiments were carried out at the SPring-8 high-energy X-ray diffraction beamline BL04B2 by using a photon energy of 61.5 keV obtained with a Si(220) monochromator. The capillaries were mounted in a furnace, and X-ray diffraction patterns were measured in transmission geometry at 358 K in the Q range (Q_{min}, Q_{max}) = (0.5, 20 $Å^{-1}$). The measured coherent scattering intensities $I(Q)$ were normalized to the Faber-Ziman X-ray weighted average structure factors $S(Q)$:

$$I(Q) = |\langle f(Q)\rangle|^2[S(Q) - 1] + \langle |f(Q)|^2\rangle \qquad (1)$$

where $f(Q)$ is the X-ray form factor and angular brackets represent averages over all atoms. Details of the data analysis can be found elsewhere.[22] The average pair distribution function (pdf) $g(r)$ was obtained via Fourier transformation of $S(Q)$ according to

$$g(r) = 1 + \frac{1}{2\pi^2\rho r}\int_{Q_{min}}^{Q_{max}} Q[S(Q) - 1]\sin(Qr)\,M(Q)\,dQ \qquad (2)$$

where ρ is the atomic number density and $M(Q)$ is a modification function introduced to reduce termination errors.[23]

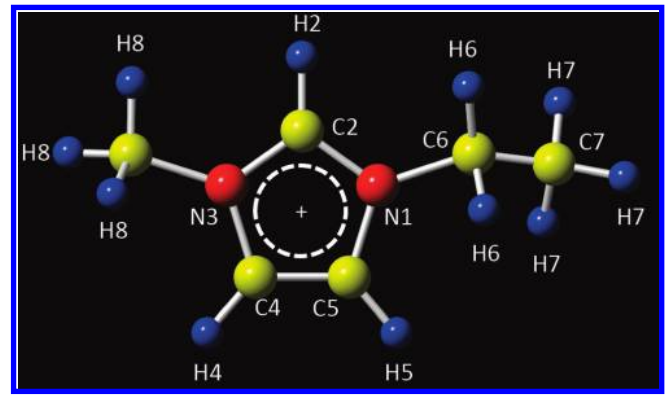

Figure 1. Structure of 1-ethyl-3-methylimidazolium cation.

Simulation Details

In order to select the best force field for studying the structure of liquid and crystalline [emim]Br, we first performed a set of geometrical optimizations by using the module in the Materials Studio 4.2 package.[24] We tested the five force fields available in Forcite in combination with four different charge distributions by performing crystal minimizations to reproduce the experimental crystal structure. The best match was obtained by combining the intramolecular and van der Waals parameters given by Dreiding[25] with the partial charges proposed by Andrade.[26] The [emim] cation is shown in Figure 1 with the atom labeling convention used here.

MD simulations were then performed by using DL_POLY 2.16.[27] A crystal structure was generated by replicating the experimental unit cell to create a supercell containing 4 × 4 × 3 unit cells and 192 pairs of $[emim]^+$ and Br^- ions. This was simulated at 300 K and 1 bar in the isobaric−isothermal (*NPT*) ensemble by using the Berendsen thermostat and barostat with relaxation constants of 1 and 5 ps, respectively.[28] A time step of 1 fs and a cutoff of 15 Å were used for the nonbonding forces, and electrostatic interactions were computed with the Ewald method and the same real-space cutoff. A simulation run of 500 ps served to determine the stability of the crystal and the corresponding lattice parameters at 300 K. The lattice parameters obtained for the equilibrated structure were $a = 8.89$ Å (+1.6%), $b = 8.12$ Å (+1.5%), $c = 12.86$ Å (+1.6%), and $\beta = 109.8°$ (−0.1%), where the values in parentheses correspond to the differences with the experimental values. The density of the simulated crystal was 1.45 g/cm^3, 4.6% lower than the experimental density. The crystal was then simulated for 100 ps in the canonical ensemble (*NVT*) with an equilibration run of 100 ps followed by a production run of 1 ns, saving the trajectory every 1 ps for further analysis. The average thermodynamic properties during the production run were $\langle T\rangle = 300 \pm 3$ K, $\langle P\rangle = 0.2 \pm 0.9$ kbar, and $\langle U\rangle = -222 \pm 1$ kJ/mol. No noticeable diffusion was observed, confirming the stability of the crystal with the force field and charges employed. The crystal

structure obtained from the simulation was compared with the crystallographic results in the literature[21] and found to be in generally good agreement.

To simulate the liquid state, we generated a disordered configuration by using the Amorphous Cell module of Materials Studio 4.2 with 125 pairs of $[emim]^+$ and Br^- ions at low density. The system was then equilibrated with DL_POLY 2.16[27] to perform a series of *NPT* simulations starting at 800 K and annealing at 700, 600, 500, 400, and 360 K. Each run lasted for 500 ps, and the final configuration corresponded to a liquid density of 1.34 g/cm^3, in good agreement with the estimate of 1.33 g/cm^3 obtained with the additivity method proposed by Ye and Shreeve.[29] The final configuration was equilibrated during 1 ns at 360 K under *NVT* conditions, followed by a production run of 3 ns where the positions were saved every 5 ps for further analysis. The thermodynamic properties obtained were $\langle T\rangle = 360 \pm 4$ K, $\langle P\rangle = -0.3 \pm 1.1$ kbar, and $\langle U\rangle = -198 \pm 1$ kJ/mol.

To confirm that our equilibration procedure led to a well-equilibrated liquid structure that did not depend on the initial configuration, a second disordered configuration was obtained by melting the crystal at 800 K and repeating the previous annealing procedure. The density obtained at 360 K was 1.35 g/cm^3, in agreement with the previous result. The structural results obtained from the analysis of this system were also in perfect agreement with those obtained previously.

Partial pdfs $g_{ab}(r)$ were calculated for each pair of inequivalent atom types (a,b) by averaging over the *NVT* ensemble and then Fourier transformed to give partial structure factors $S_{ab}(Q)$. X-ray weighted average structure factors $S(Q)$ were calculated by taking into account the form factor and concentration of each atom type. Finally, average pdfs $g(r)$ were calculated with eq 2 with the same procedure as that used for the X-ray data. Although the charges used in the simulation correspond to a charge of $+1$ and -1 on the $[emim]^+$ cation and Br^- anion, respectively, it should be kept in mind that there is not necessarily complete charge transfer in ionic systems and that the average structure factor may be modified as a result.[30]

Results and Discussion

The simulated and measured average structure factors $S(Q)$ are shown in Figure 2, together with the intramolecular and intermolecular contributions obtained from the simulation. The experimental $S(Q)$, dominated by the intense peak at $Q \approx 1.7$ Å^{-1} with a small shoulder at $Q \approx 1.1$ Å^{-1}, presents some similarities with that of $[emim]BF_4$:[20] in both cases, the first peak is followed by a second peak slightly below 4 Å^{-1}, a third one close to 6 Å^{-1}, and some less well-defined oscillations beyond. The $S(Q)$ is significantly different from the RTIL liquid formed by the $[emim]^+$ cation and the more complex bis-(trifluoromethanesulfonyl)imide anion.[19] The simulation reproduces the main experimental features quite well, including the shoulders on either side of the main peak.

The corresponding pdfs shown in Figure 3 are also in good agreement, although the simulation overemphasizes somewhat the intramolecular structure. The simulation reproduces reasonably well the pronounced peaks observed experimentally at ~3.7, ~4.8, and ~5.6 Å, although some differences appear between 4 and 4.6 Å. The pdf shows small but clear oscillations up to 14 Å (inset to Figure 3), consistent with the strong main peak in $S(Q)$.

To identify the origin of the observed peaks, we calculated the partial contributions to the average pdf. Figure 4 shows the five partial pdfs involving the Br^- anion and the N, C (sp^2), C(sp^3), H, and Br atoms, which contribute 60% to the total pdf. The sum of these weighted partials shows the same features as the average pdf. The close H−Br contacts produce the peak at 2.9 Å. The remaining features cannot be assigned to a single partial pdf, but the main contributions to the first peak at 3.7 Å come from the contacts between Br and C atoms, either those of the ring or those in the methyl and ethyl chains. Although the Br−Br partial pdf has a broad first peak extending from 5 to 9.5 Å with a maximum around 6−7 Å, the total pdf has instead a dip at this distance due to the minima found in other important contributions such as N−Br and C−Br.

In Figure 5, we compare the simulated intermolecular pdfs of crystal and liquid. As expected, only the crystal shows well-defined order beyond 14 Å. However, the first few features below 6 Å present remarkable similarities between crystal and liquid. In particular, the position and intensity of the first, second, and fourth peaks largely coincide. The main difference appears at the third peak, which is much weaker in the liquid and shifted to higher *r*. To compare in more details the ordering of the anions around the $[emim]^+$ cation, Figure 6 shows the partial pdfs between the Br^- ion and the atoms on the cation for the

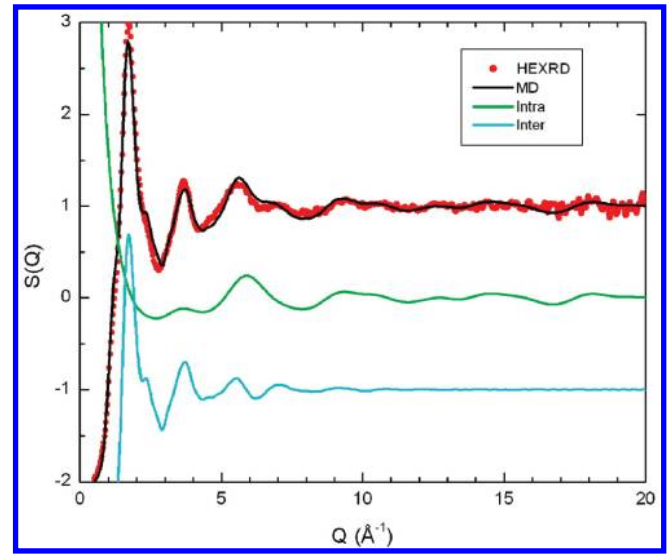

Figure 2. X-ray weighted average structure factors obtained from the HEXRD experiment and MD simulations. The simulated intra- and intermolecular contributions are also shown.

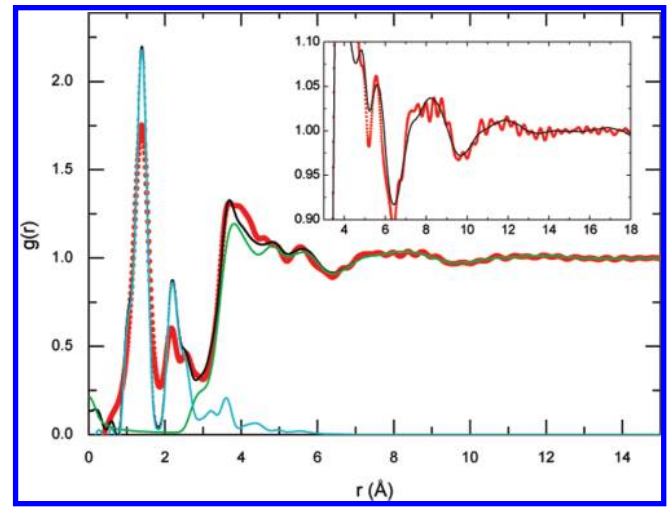

Figure 3. X-ray weighted average pdfs obtained from the HEXRD experiment and MD simulations. The intra- and intermolecular contributions to the latter are also shown. Same notation as in Figure 2. The inset shows an enlargement of the long-range oscillations.

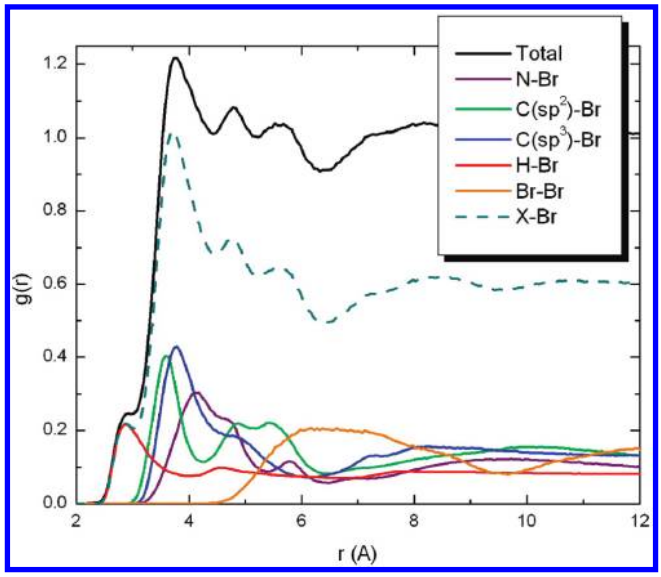

Figure 4. Contributions of the different atom pairs to the intermolecular pdfs from the MD simulations. The black line shows the total pdf, and the dashed line shows the sum of the partial pdfs involving Br.

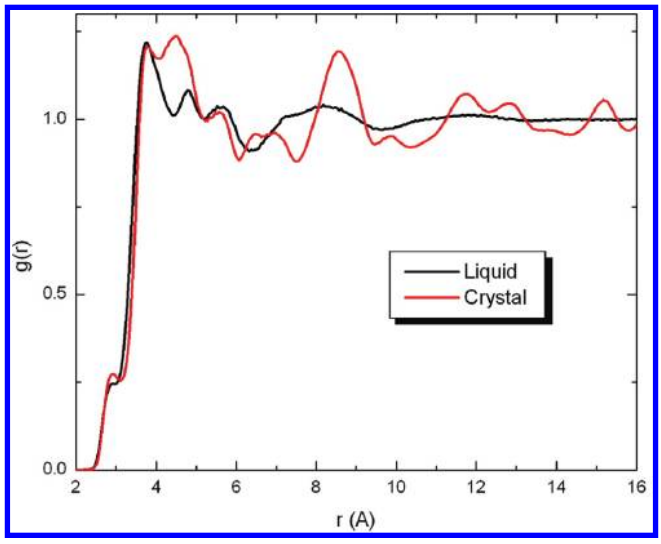

Figure 5. Intermolecular pdfs for the liquid and the crystal.

liquid and the crystal. The correlations of Br^- with the atoms of the ethyl (C6, C7, H6, H7) and methyl groups (C8, H8) are very similar in the two phases, as are those with the H atoms of the ring (H2, H4, H5), although, in this case, the long-range order of the crystal is clearly manifested by the well-defined oscillations beyond the first peak, which are clearly damped in the liquid. Only in the case of H2 is the first peak significantly broader in the liquid. The correlations with the carbon atoms in the ring (C2, C4, C5) indicate a shift of the first peak to shorter distances in the liquid. Although this shift is quite small for C4, it is noticeably larger for C5 and in particular for C2. It is also interesting to note that, although the similarity of the C2 and C4 correlations between liquid and crystal extends to the second coordination cell, this is not the case for the C5, for which the intense second peak around 4.5 Å in the crystal is damped in the liquid and shifted to larger *r*. The N1 correlation is again quite similar for both phases, but the N3 shows a broad peak in the crystal that is split into two peaks for the liquid: the one at shorter *r* indicates significantly closer Br^-−N3 contacts in the liquid, like for the Br^-−C2 and Br^-−C5 pairs. The difference between liquid and crystal in the third peak of the

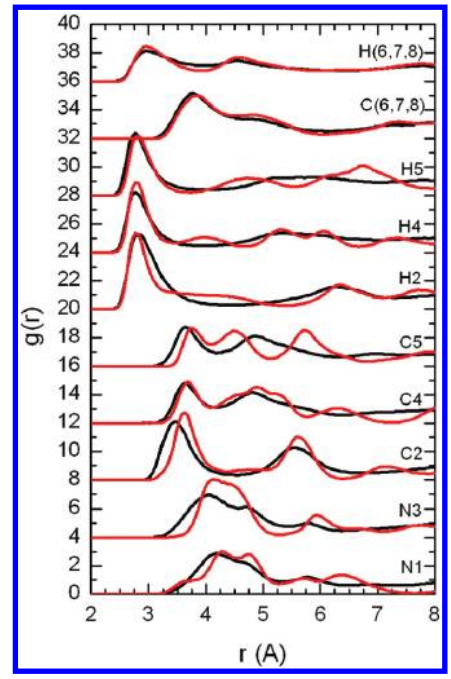

Figure 6. Partial Br−X pdfs for liquid (black) and crystal (red).

total pdf (Figure 5) is due mainly to the reduced intensity of the Br^-−N3 and Br^-−C5 partials in the liquid in this region. Overall, the distribution of Br^- anions around the [emim] cation exhibits significant similarities between the liquid and the crystal but with two important differences: the anions are distributed more symmetrically around the ring in the liquid and approach the ring atoms more closely.

To visualize the general ordering of cations and anions in the system, Figure 7a shows three partial pdfs representing the correlations between the geometrical centers of the imidazolium rings (RC) and the Br anions. The three partials for the liquid, shown in the inset, clearly exhibit the charge ordering typical of ionic liquids, extending beyond the maximum distance of the simulation, 18 Å. The first and most intense peak, appearing at 4.6 Å, corresponds to the cation−anion correlations. The RC−BR pdf exhibits a second well-defined peak at 5.9 Å, overlapping the first peak of the Br−Br pdf. Although the RC−Br pdf exhibits a well-defined first coordination shell, similar to that observed in the crystal, this is not the case for the RC−RC and Br−Br liquid pdfs. Both exhibit very broad features, and no clear coordinations shells can be identified. The most interesting feature is the shoulder in the RC−RC pdf at low *r,* indicating that some imidazolium rings are arranged in such a way that their centers come as close as 3.5 Å, much nearer than in the crystal.

The coordination number on the first shell of Br^- ions around a cation in the liquid is about four and goes up to six if the integration is extended over the second peak. The coordination number of the crystal is also six if the integration is taken up to 6.1 Å. Regarding the RC−RC correlations, the first neighbor in the liquid is always at a distance below 5.2 Å, whereas on the crystal, the coordination number of one is only reached at 5.45 Å.

The corresponding partial structure factors are shown in Figure 7b. The dominant peak in the liquid structure factor at 1.7 $Å^{-1}$ appears in all the RC−RC, Br−Br, and RC−Br partial structure factors and can be associated with the topological short-range order, characterized by the mean RC−Br^- distance of 4.5 Å. In contrast, the small shoulder around 1.1 $Å^{-1}$ results

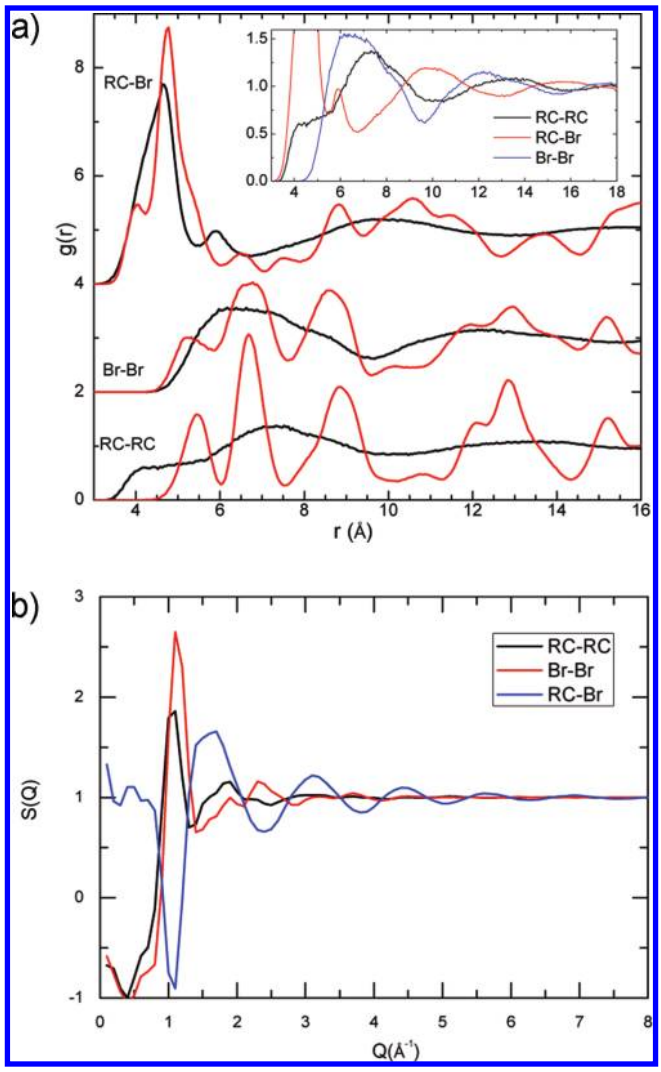

Figure 7. (a) Partial pdfs corresponding to correlations between the centers of two imidazolium rings (RC−RC), the center of one ring and one Br atom (RC−Br), and two anions (Br−Br) in the crystal (red) and liquid (black). The inset shows the three pdfs for the liquid superimposed. (b) Corresponding partial structure factors obtained from MD simulations.

from large, sharp positive peaks in the RC−RC and Br−Br partial structure factors and a corresponding negative peak in the RC−Br partial structure. This behavior is typical of the Coulomb short-range order generally found in molten salts. Finally, the three partial structure factors also show a small feature around 0.5 Å^{-1} that is too small to be apparent in the average $S(Q)$, indicating a small degree of intermediate-range order.[31]

To determine the extent of orientational order in the arrangement of the bulky cations, their relative orientation distributions is plotted in Figure 8 for different separation distances. The angle θ is subtended by the two vectors perpendicular to the ring plane of each cation, in a direction defined, for example, as going into the plane of Figure 1. In the crystal structure measured by Elaiwi et al.,[21] the two closest pairs of [emim]$^+$ cations are at distances of 5.4 and 5.65 Å, with their planes forming angles of 60 and 0°, respectively. Further pairs oriented at 60° appear at 6.6 and 8.7 Å, whereas parallel pairs are at 7.6, 8.0, and 8.7 Å. As shown in Figure 8, in the simulated crystal, we observe a broadening of these distributions and a shift of the first down to 40°. In the liquid, pairs of closely approaching rings adopt either a parallel or an antiparallel

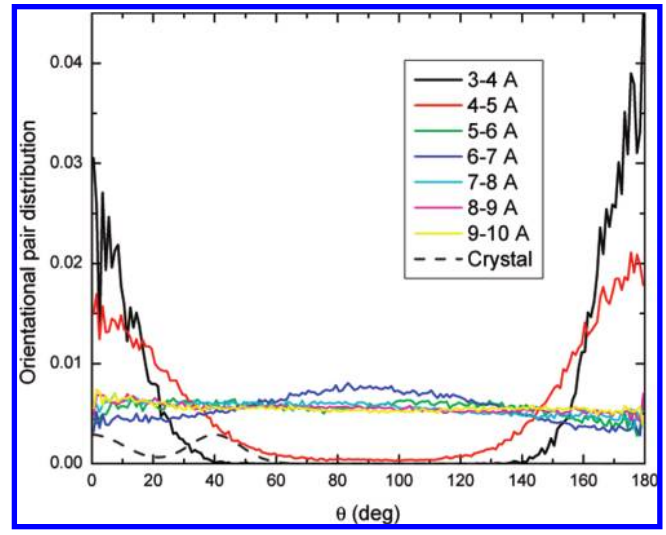

Figure 8. Distributions of the population of [emim] pairs as a function of their relative orientation for different separation distances. The histograms have been divided by the factor sin θ and normalized by the total number of pairs found at each range of distances.

configuration, with a slight preference for the latter. For pairs separated by less than 4 Å, the distribution peaks strongly at 0 and 180° with no pairs found with angles deviating from those values by more than 40°. A similar result is obtained for pairs having a separation distance in the range between 4 and 5 Å; but now, the distribution is broader, and there is a small number of pairs with a perpendicular orientation. For distances beyond 5 Å, the distribution becomes almost flat; but for pairs separated by a distances of 6−7 Å, a broad maximum is observed around 90°, suggesting a slight preference for perpendicular alignment. For all distances larger than 7 Å, the flat distribution is recovered, indicating a totally random orientation of the cation pairs.

Conclusions

The main features revealed by the combined HEXRD experiments and MD simulations can be summarized as follows. The dominant peak in the liquid structure factor at 1.7 Å^{-1} appears in all the RC−RC, Br−Br, and RC−Br partial structure factors and can be associated with the topological short-range order, characterized by the mean RC−Br$^-$ distance of 4.5 Å. In contrast, the small shoulder around 1.1 Å^{-1} results from large, sharp positive peaks in the RC−RC and Br−Br partial structure factors and a corresponding negative peak in the RC−Br partial structure, a behavior typical of charge ordering in molten salts.

The intermolecular part of the pair distribution function is characterized by peaks at 3,7, 4.8, and 5.6 Å, all involving correlations of Br$^-$ with other atoms, either Br$^-$ itself or atoms on the cation. At short distances, there are clear similarities in the total pdf between the liquid and the crystal, except for the 4.8 Å peak, which is lower and shifts to larger r in the liquid, mainly as a consequence of reduced N3−Br and C5−Br interactions. At the same time, the correlations between Br and all five ring atoms show increasing intensity at low r in the liquid. Overall, the Br atoms become more symmetrically distributed around the ring, and some move closer to the ring atoms. This is confirmed by the analysis of the distributions of cations and anions presented in Figure 7a. Clear similarities between liquid and crystal are observed in the RC−Br pdf, with less asymmetry in the liquid, whereas the cation−cation and anion−anion correlations show marked differences between the

liquid and crystal. This is particularly striking in the RC−RC correlation function, which exhibits a significant shift to lower r in the liquid, with some pairs coming as close as 3.5 Å. Analysis of the angular correlations in the MD results shows that these close pairs adopt either a parallel or antiparallel configuration, with a slight preference for the latter. The angular correlations become less marked as the distances between centers increases and are almost completely random at a separation of 7 Å.

Acknowledgment. The HEXRD experiments were carried out at the High-Energy X-ray Diffraction Beamline BL04B2 at the Japan Synchrotron Radiation Research Institute, SPRing-8, Hyogo, Japan. The authors are grateful to Drs. David Price and Felix Fernandez-Alonso for helpful discussions. This work was supported jointly by the Institut de Physique INP, CNRS (Paris) and by the Institut Laue Langevin (Grenoble).

References and Notes

(1) Wasserscheid, P., Welton, T., Eds. *Ionic Liquids in Synthesis*; Wiley-VCH: Weinheim, 2003.
(2) Weingärtner, H. *Angew. Chem., Int. Ed.* **2008**, *47*, 654–670.
(3) Maginn, E. J. *J. Phys.: Condens. Matter* **2009**, *21*, 373101.
(4) Hunt, P. A. *Mol. Simul.* **2006**, *32*, 1–10.
(5) Hardacre, C.; Holbrey, J. D.; McMath, S. E. J.; Bowron, D. T.; Soper, A. K. *J. Chem. Phys.* **2003**, *118*, 273–278.
(6) Hardacre, C.; McMath, S. E. J.; Nieuwenhuyzen, M.; Bowron, D. T.; Soper, A. K. *J. Phys.: Condens. Matter* **2003**, *15*, S159–S166.
(7) Deetlefs, M.; Hardacre, C.; Nieuwenhuyzen, M.; Padua, A. A. H.; Sheppard, O.; Soper, A. K. *J. Phys. Chem. B* **2006**, *110*, 12055–12061.
(8) Hamaguchi, H.; Ozawa, R. *Adv. Chem. Phys.* **2005**, *131*, 85–104.
(9) Katayanagi, H.; Hayashi, S.; Hamaguchi, H.; Nishikawa, K. *Chem. Phys. Lett.* **2004**, *392*, 460–464.
(10) Hagiwara, R.; Matsumoto, K.; Tsuda, T.; Ito, Y.; Kohara, S.; Suzuya, K.; Matsumoto, H.; Miyazaki, Y. *J. Non-Cryst. Solids* **2002**, *312−314*, 414–418.
(11) Matsumoto, K.; Hagiwara, R.; Ito, Y.; Kohara, S.; Suzuya, K. *Nucl. Instrum. Methods Phys. Res., Sect. B* **2003**, *199*, 29–33.
(12) Triolo, A.; Mandanici, A.; Russina, O.; Rodriguez-Mora, V.; Cutroni, M.; Hardacre, C.; Nieuwenhuyzen, M.; Bleif, H.-J.; Keller, L.; Ramos, M. A. *J. Phys. Chem. B* **2006**, *110*, 21357–21364.
(13) Holbrey, J. D.; Reichert, W. M.; Nieuwenhuyzen, M.; Johnston, S.; Seddon, K. R.; Rogers, R. D. *Chem. Commun.* **2003**, 1636–1637.
(14) Urahata, S. M.; Ribeiro, M. C. C. *J. Chem. Phys.* **2004**, *120*, 1855–1863.
(15) Wang, Y.; Voth, G. A. *J. Am. Chem. Soc.* **2005**, *127*, 12192–12193.
(16) Canongia Lopes, J. N. A.; Padua, A. A. H. *J. Phys. Chem. B* **2006**, *110*, 3330–3335.
(17) Triolo, A.; Russina, O.; Bleif, H.-J.; Di Cola, E. *J. Phys. Chem. B* **2007**, *111*, 4641–4644.
(18) Takahashi, S.; Suzuya, K.; Kohara, S.; Koura, N.; Curtiss, L. A.; Saboungi, M.-L. *Z. Phys. Chem.* **1999**, *209*, 209–221.
(19) Fujii, K.; Soejima, Y.; Kyoshoin, Y.; Fukuda, S.; Kanzaki, R.; Umebayashi, Y.; Yamaguchi, t.; Ishiguro, S.; Takamuku, T. *J. Phys. Chem. B* **2008**, *112*, 4329–4336.
(20) Kanzaki, R.; Mitsugi, T.; Fukuda, S.; Fujii, K.; Takeuchi, M.; Soejima, Y.; Takamuku, T.; Yamaguchi, T.; Umebayashi, Y.; Ishiguro, S. *J. Mol. Liq.* **2009**, *147*, 77–82.
(21) Elaiwi, A.; Hitchcock, P. B.; Seddon, K. R.; Srinivasan, N.; Tan, Y.-M.; Welton, T.; Zora, J. A. *J. Chem. Soc., Dalton Trans.* **1995**, 3467–3472.
(22) Kohara, S.; Takata, M.; Matsumoto, K.; Hagiwara, R.; Suzuya, K.; Morita, H.; Siewenie, J. E.; Benmore, C. J. *J. Chem. Phys.* **2008**, *129*, 014512.
(23) Lorch, E. *J. Phys. C: Solid States Phys.* **1969**, *2*, 229.
(24) *Materials Studio Modelling Environment*, version 4.2; Accelrys Inc.: San Diego, 2007.
(25) Mayo, S. L.; Olafson, B. D.; Goddard, W. A., III. *J. Phys. Chem.* **1990**, *94*, 8897–8909.
(26) Andrade, J.; Böes, E. S.; Stassen, H. *J. Phys. Chem. B* **2002**, *106*, 3546–3548.
(27) Smith, W.; Young, C. W.; Rodger, P. M. *Mol. Simul.* **2002**, *28*, 385–471.
(28) Berendsen, H. J. C.; Postma, J. P. M.; van Gunsteren, W.; DiNola, A.; Haak, J. R. *J. Chem. Phys.* **1984**, *81*, 3684.
(29) Ye, C.; Shreeve, J. M. *J. Phys. Chem. A* **2007**, *111*, 1456–1461.
(30) Badyal, Y. S.; Saboungi, M.-L.; Price, D. L.; Haeffner, D. R.; Shastri, S. D. *Europhys. Lett.* **1997**, *39*, 19–24.
(31) Price, D. L.; Moss, S. C.; Reijers, R.; Saboungi, M. L.; Susman, S. *J. Phys: Condens. Matter* **1989**, *1*, 1005–1008.

JP1070715